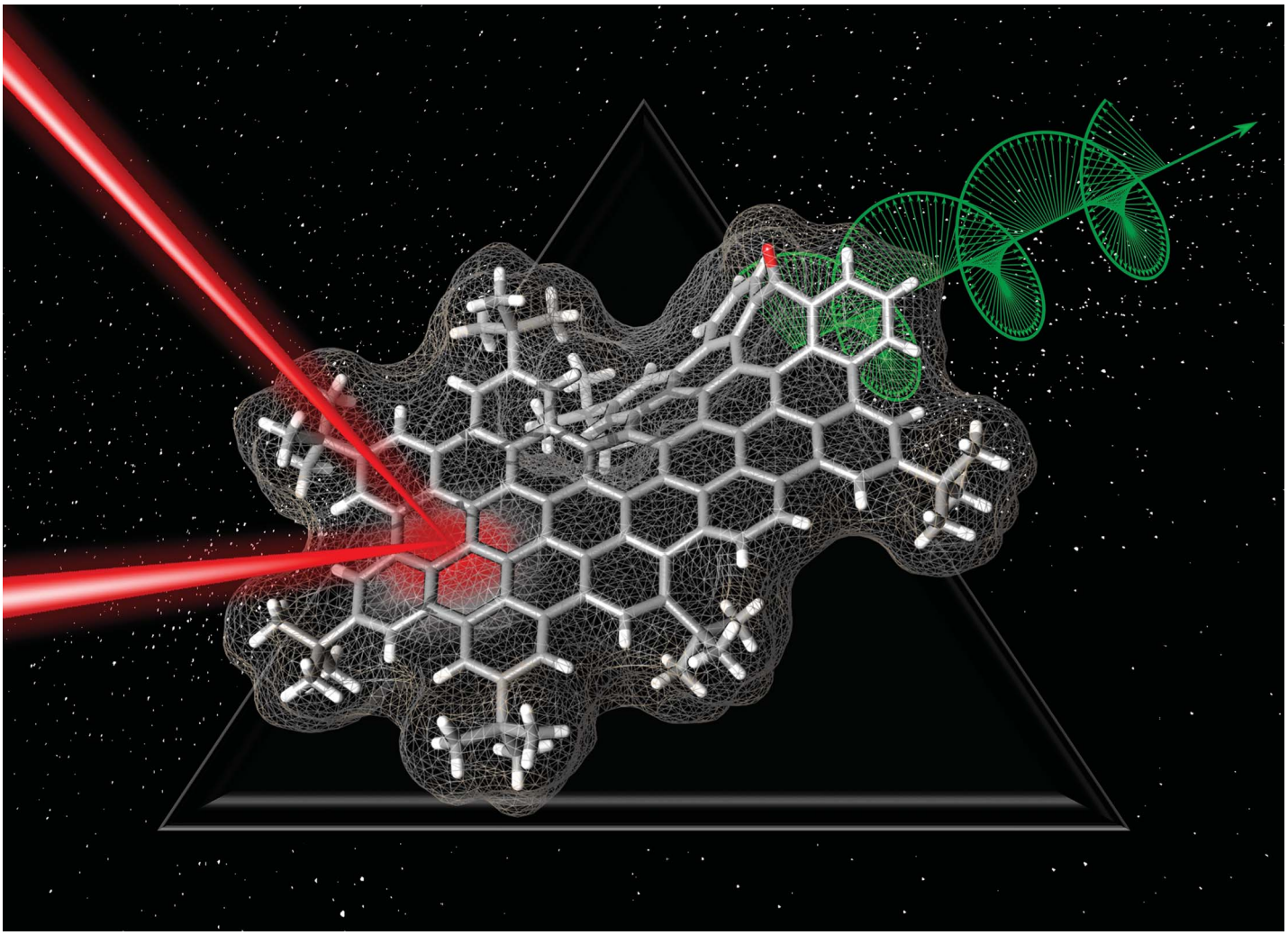

Showcasing research from Dr Araceli Campaña's laboratory, Organic Chemistry, University of Granada, Granada, Spain.

Enantiopure distorted ribbon-shaped nanographene combining two-photon absorption-based upconversion and circularly polarized luminescence

A distorted ribbon-shaped nanographene exhibits an unprecedented combination of optical properties in graphene-related materials, namely upconversion based on two-photon absorption (TPA-UC) together with circularly polarized luminescence (CPL).

As featured in:

See Ermelinda Maçôas, Araceli G. Campaña *et al.*, *Chem. Sci.*, 2018, **9**, 3917.

ROYAL SOCIETY OF CHEMISTRY

rsc.li/chemical-science

Registered charity number: 207890

Chemical Science

EDGE ARTICLE

View Article Online
View Journal | View Issue

Cite this: *Chem. Sci.*, 2018, **9**, 3917

Enantiopure distorted ribbon-shaped nanographene combining two-photon absorption-based upconversion and circularly polarized luminescence†

Carlos M. Cruz,[a] Irene R. Márquez,[a] Inês F. A. Mariz,[b] Victor Blanco,[a] Carlos Sánchez-Sánchez,[c] Jesús M. Sobrado,[d] José A. Martín-Gago,[cd] Juan M. Cuerva,[a] Ermelinda Maçôas *[b] and Araceli G. Campaña *[a]

Received 26th January 2018
Accepted 7th March 2018

DOI: 10.1039/c8sc00427g

rsc.li/chemical-science

Herein we describe a distorted ribbon-shaped nanographene exhibiting unprecedented combination of optical properties in graphene-related materials, namely upconversion based on two-photon absorption (TPA-UC) together with circularly polarized luminescence (CPL). The compound is a graphene molecule of *ca.* 2 nm length and 1 nm width with edge defects that promote the distortion of the otherwise planar lattice. The edge defects are an aromatic saddle-shaped ketone unit and a [5]carbohelicene moiety. This system is shown to combine two-photon absorption and circularly polarized luminescence and a remarkably long emission lifetime of 21.5 ns. The [5]helicene is responsible for the chiroptical activity while the push–pull geometry and the extended network of sp^2 carbons are factors favoring the nonlinear absorption. Electronic structure theoretical calculations support the interpretation of the results.

Introduction

Defect engineering in graphene-like materials can be an interesting approach to tune their remarkable electronic and optical properties.[1] An illustrative example is that of graphene quantum dots (GQDs), in which the fluorescence emission quantum yields are strongly dependent upon the presence of defects,[2] and the high two-photon absorption (TPA) cross-section values recently reported have been mostly associated with doped GQD.[3] The photon upconversion process that follows from high emission yields combined with TPA in organic materials has been explored in many applications including three-dimensional (3D) data storage, 3D-microfabrication, up-converted lasing, sensing, theragnostics and bioimaging.[4] Nevertheless, the preparation of GQD is usually based on methods that lead to heterogeneous materials, lacking control over the final structure and fostering an intense debate over the origin of their optical response.[5] The controlled introduction of defects in carbon nanomaterials is only possible if suitable synthetic routes to produce such defects are available, allowing the preparation of homogenous and well-defined materials. Within this context, bottom-up approaches to carbon-based nanostructures are essential.[6] For instance, the reported synthesis of structurally well-defined graphene nanoribbons (GNRs) produces a defined and tunable band gap relevant for optical properties.[7] Graphene molecules or nanographenes, graphene fragments from 1 nm in size,[6d] have been seen as useful models in the study of carbon-based nanostructures. Chiral carbon nanostructures are also of increasing interest and their chiroptical properties are being extensively studied.[8] In this work, we hypothesize that the controlled introduction of defects in nanographenes (Fig. 1) can implement interesting new combinations of optical properties, such as TPA-based upconversion (TPA-UC) and circularly polarized luminescence (CPL). Remarkably, to the best of our knowledge, the combination of both responses in a single organic molecule has never been addressed although it would represent the foundation for the development of TPA-based UC-CPL.[9]

In this sense, large π-conjugated linkers between donor–acceptor moieties are basic structural features required for two-photon absorbing chromophores.[10] On the other hand, chiral molecules able to produce circular polarized luminescence

[a]*Departamento Química Orgánica, Universidad de Granada (UGR), C. U. Fuentenueva, 18071 Granada, Spain. E-mail: araceligc@ugr.es*

[b]*Centro de Química-Física Molecular (CQFM), Institute of Nanoscience and Nanotechnology (IN) and Centro de Química Estrutural, Instituto Superior Técnico, University of Lisbon, Av. Rovisco Pais, 1, 1049-001 Lisboa, Portugal*

[c]*Instituto de Ciencia de Materiales de Madrid (ICMM-CSIC), Sor Juana Inés de la Cruz 3, 28049 Madrid, Spain*

[d]*Centro de Astrobiología INTA-CSIC, Torrejón de Ardoz, 28850 Madrid, Spain*

† Electronic supplementary information (ESI) available: General details, synthesis and spectroscopy data of new compounds. Experimental details on optical, chiroptical, electrochemical and on-surface measurements. Crystal data and structure refinement of compounds **1**, and **6**. Further details on theoretical calculations and Cartesian coordinates of computed structures. VT-H^1NMR, 2D-NMR and HRMS spectra of **1**. CCDC 1561552 and 1561553. For ESI and crystallographic data in CIF or other electronic format see DOI: 10.1039/c8sc00427g

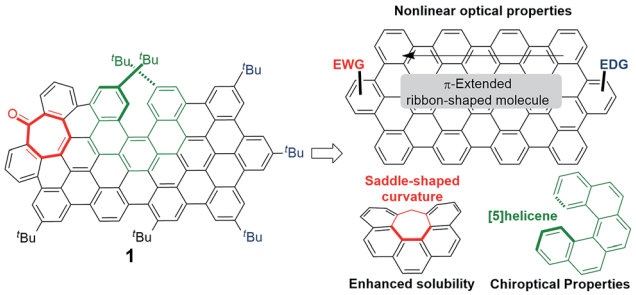

Fig. 1 Key structural features (right) present in the target distorted ribbon-shaped graphene molecule **1** (left).

(CPL)[11] responses are of increasing interest due to their promising applications in optical devices and biosensors.[12]

Organic molecules with π-conjugated structures and chiral moieties such helicenes or binaphtyls have been extensively reported as CPL-active compounds.[13] Nevertheless, the CPL of an enantiopure nanographene remains still unexplored.

Bearing all these ideas in mind, enantiopure defective ribbon-shaped graphene molecule **1** (Fig. 1) was synthesized, showing both TPA-based upconversion and CPL response.

Distorted nanographene **1** combines three key structural features. Firstly, we chose the required electron withdrawing unit as a carbonyl group introduced in the hexagonal network as a tropone moiety in a heptagon-containing polycyclic arene.[14] Thus, the incorporation of heptagons in ribbon-shaped conjugated molecules causes deep distortions away from planarity, going from rigid structures with low solubility to contorted, flexible and soluble systems,[14f,i] favouring an adequate purification and characterization and modifying also the electronic and optical properties of final compounds.[15] Moreover, the seven-membered ring facilitates the easy introduction of an acceptor group avoiding aryl substituents that would deactivate the final synthetic oxidation step. The central electron rich π-extended aromatic network is also essential for reasonable TPA responses. Finally, a non-racemizable [5]helicene moiety[16] introduced in the aromatic network would act as the enantiopure motif inducing a chiroptical response. Moreover, the synergetic effect of the saddle-shaped curvature induced by the heptagon together with the helicity caused by the [5]helicene might avoid the establishment of π,π-interactions between molecules, enhancing solubility and processability in organic solvents.

Results and discussion

Synthetic methodology and structural analysis

Bringing together all the structural requirements in one single molecule requires a fine control over the synthetic procedure. We recently reported a straightforward synthesis of heptagon-containing PAHs.[17] Since this method allows the preparation of distorted PAHs and the versatile incorporation of functional groups in selected positions, we used it to create an aromatic backbone incorporating a π-extended helical moiety in the structure (Scheme 1a).[18,19]

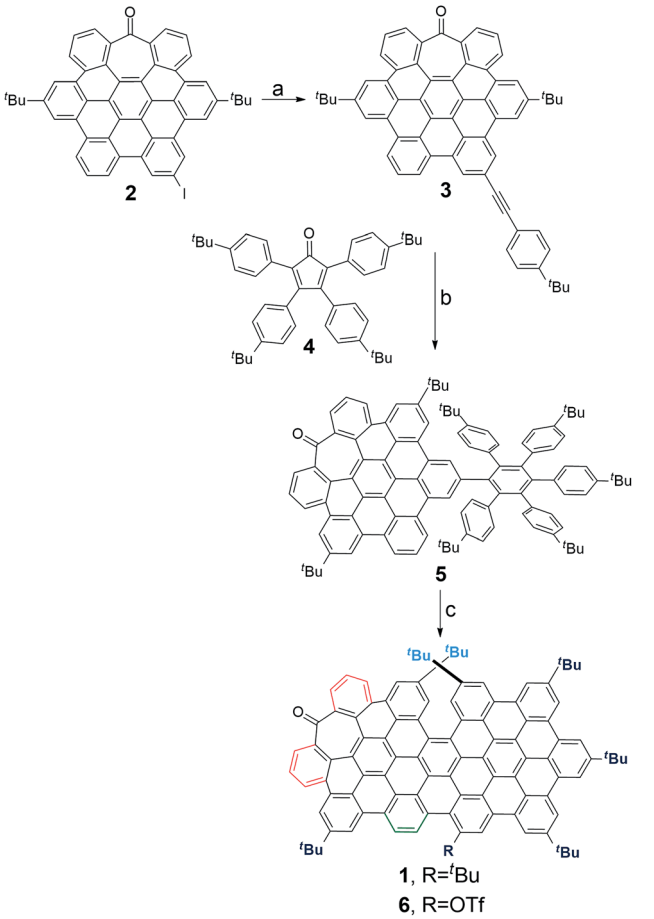

Scheme 1 Synthesis of compound **1**. Reagents and conditions: (a) 4-*tert*-butylphenylacetylene, $PdCl_2(PPh_3)_2$, CuI, NEt_3, THF, RT, 16 h, 99%; (b) Ph_2O, reflux, 8 h, 34%; (c) DDQ, CF_3SO_3H, CH_2Cl_2, 0 °C, 10 min, **1** (46%) and **6** (5%).

Starting from the previously reported heptagon-containing distorted nanographene **2**,[17] Sonogashira coupling with *p-tert*-butylphenylacetylene afforded **3** in a quantitative yield. Subsequent Diels–Alder reaction with cyclopentadienone **4** gave polyphenylene **5** in a moderate 34%. Final oxidative cyclodehydrogenation reaction with a DDQ/TfOH mixture in CH_2Cl_2 at 0 °C yielded orange solid **1** as a major product (46%). In this final step, we also isolated a minor amount of triflate derivative **6** (5%).

Compound **1** was firstly characterized by MALDI-TOF, where there is only one dominant peak in the mass spectrum of **1** and the isotopic distribution pattern of the high-resolution mass peak is in good agreement with the calculated pattern (Fig. 2b). Remarkable good solubility of **1** in organic solvents ($CHCl_3$, CH_2Cl_2, dichloroethane, tetrachloroethane, acetone, THF, and to some extent even in hexane) allowed us to undertake its structure determination also by means of ^{1}H-NMR spectroscopy (Fig. 2a), both techniques confirming the proposed structure.

Additionally, slow methanol vapor diffusion into a chlorobenzene solution of **1** allowed the growing of diffraction-quality single crystals. X-ray crystallography revealed the structure of **1** with a distorted conformation of the aromatic backbone (Fig. 3).[20]

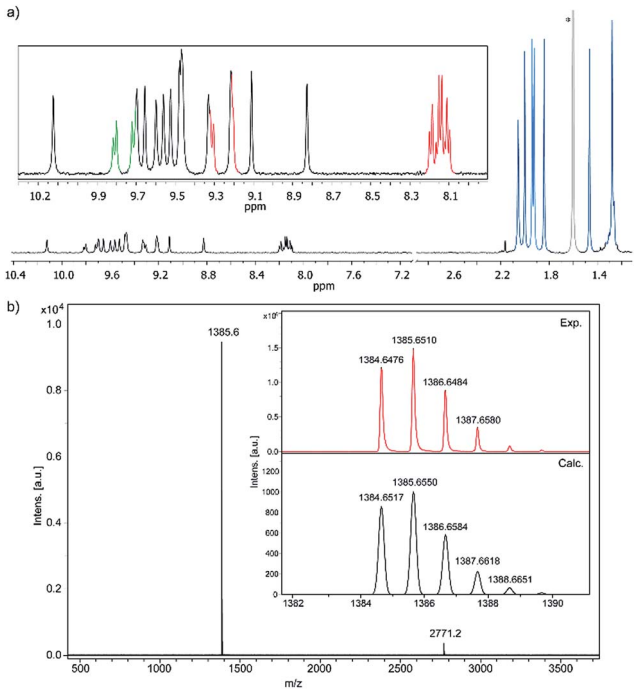

Fig. 2 (a) Partial ^{1}H-NMR spectra (500 MHz, $C_2D_2Cl_4$, 293 K) of **1** (see color code in Scheme 1) *this signal corresponds to residual water. (b) MS and HR-MS (MALDI-TOF) of **1**.

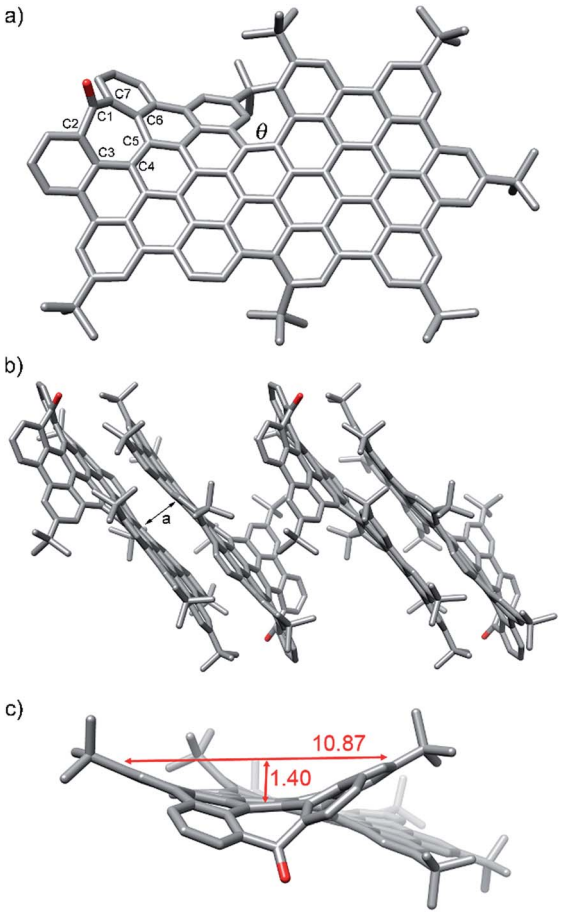

Fig. 3 X-Ray crystal structure of **1**: (a) top view, selected bond lengths (Å): C1–C2, 1.466; C2–C3, 1.422; C3–C4, 1.482; C4–C5, 1.432; C5–C6, 1.486; C6–C7, 1.407; C1–C7, 1.464; (b) molecular packing, π–π distance (a): *ca.* 3.4–3.5 Å; (c) front view showing the dimensions (in Å) of the aromatic saddle-shaped region. Hydrogen atoms and solvent molecules have been omitted for clarity.

As a chiral molecule, **1** exists as a pair of enantiomers in the crystals. Fig. 3a shows the *P* enantiomer. As expected, the inclusion of the heptagon causes a saddle-shaped curvature in the hexagonal network, that is 10.8 Å wide and 1.4 Å deep (Fig. 3c), reaching deviation from planarity with angles of up to 24° between the mean plane of the aromatic ring next to the heptagon and the mean plane of the hexagonal planar region (see ESI, Table S4†). The molecular packing shows the presence of π-stacking of **1** to form groups of two stacked molecules with a π–π distance of *ca.* 3.4–3.5 Å. These dimers do not establish π–π interactions among them and are separated by layers of disordered solvent molecules. Within each pair, the molecules are arranged antiparallelly, interacting mainly through the planar regions on the non-defective side. The [5]helicene moieties are pointing towards the face that does not participate in π-stacking interactions. The molecules are displaced in such a way that the area around the 7-membered rings and the [5]helicene moieties are located outside the interaction region. The C–C bond lengths observed in the seven-membered ring indicate localization of π-bonds corresponding to a 2,4,6-cycloheptatrien-1-one or tropone unit with C–C single bonds between sp^2–sp^2 carbons, similarly to previously reported aromatic saddles (Fig. 3).[14i]

It is noteworthy that the twisted conformation caused by the [5]helicene moiety difunctionalized with ^{t}Bu groups originates a torsion angle (θ) of *ca.* 30°, the highest ever reported to date for a [5]helicene.[16] This distortion from planarity enhances solubility avoiding strong π,π-interactions between molecules. Thus, despite the large π-surface constituted by 25 aromatic rings, with a C–C length of *ca.* 1.98 nm and C–C width of *ca.* 0.98 nm, **1** shows a solubility of up to 16 mg mL^{-1} in CH_2Cl_2.

Linear and non-linear optical properties

The optical properties of **1** were determined by one-photon absorption (OPA) and TPA spectroscopy in the UV-vis and NIR regions and emission spectroscopy with linear and nonlinear excitation (Fig. 4). The UV-vis spectrum of **1** in the 300–800 nm region reveals a structured absorption band between 400 and 500 nm with a maximum at 444 nm (OPA) (Fig. 4a, black line). The corresponding molar absorptivity was estimated to be of 6.6 $\times$ 10^4 M^{-1} cm^{-1}. Based on TD-DFT calculations (see ESI, Table S5†), this structured band is composed of three different transitions predicted at 507, 464 and 449 nm in good agreement with the observed peaks at 493, 475 and 444 nm, respectively. Additional contribution from the typical vibronic progression of rigid aromatic systems to the band structure cannot be completely ruled out. The lowest energy $S_0 \rightarrow S_1$ transition, calculated at 527 nm, is observed as a very weak band at 555 nm in agreement with its predicted weak oscillator strength. This band is only clearly observed in more concentrated solutions (10^{-5} M, inset, Fig. 4a). The assignment of this band to the monomer is also supported by its observation on the

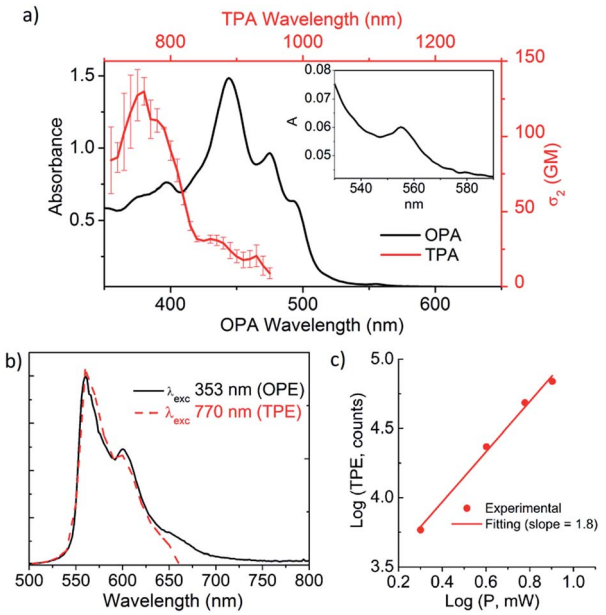

Fig. 4 (a) Two-photon and one-photon absorption (TPA and OPA) of **1** in CH_2Cl_2 (inset: OPA of **1** in the 530–590 nm region at 10^{-5} M in CH_2Cl_2); (b) two-photon induced emission (TPE) upon excitation at 770 nm and one-photon induced emission (OPE) upon excitation at 353 nm and (c) log–log plot of the photon counts from TPE as a function of the excitation power. A slope of 1.8 is indicative of the quadratic dependence of the emission on the excitation power. In plot (a) the TPA is shown using a wavelength scale that is twice the one of the OPA. The emission spectra are normalized and were recorded with solutions of **1** of *ca.* 2×10^{-6} M.

photoluminescence excitation spectrum collected at 600 nm (see ESI, Fig. S18†).

The emission spectrum of **1** (one-photon excitation, OPE) (Fig. 4b, black line) consists of three major vibronic bands at 560, 601 and 649 nm with decreasing intensities as the wavelength increases. The vibronically resolved emission spectrum is typical of rigid aromatic fluorophore.[21] The difference between consecutive bands in the progression is consistent with the coupling of the electronic transition with ring breathing modes observed in the 1250 cm^{-1} region (see ESI, Fig. S13†). The fluorescence quantum yield (ϕ_F) is 13%. The excitation independent emission and an overlapping between the absorption and excitation spectra indicate that the sample is homogeneous and has neither impurities nor aggregates. The optical band gap estimated from the curve crossing of the normalized absorption and emission spectra is 2.22 eV. The emission lifetime was measured at two different wavelengths, at the maximum and the red edge of the emission band, showing a very small wavelength dependence. Emission lifetime is multiexponential (25.6, 18.1 and 3.5 ns) with the major contribution (68%) coming from the longest time-constant.

The different lifetimes might be due to the relaxation pathways involving the two different saddle-to-saddle diastereoisomers that are rapidly interchanging at the fluorescence timescale. The average fluorescence lifetime is $\tau = 21.5$ ns, significantly longer than that of related fluorescent dyes, such as perylene bisimides.[22]

As anticipated based on its push–pull geometry with an extended aromatic network connecting the electron acceptor heptagon unit to the electron donating ^{t}Bu groups and the calculated dipole moment of 4.64 D, **1** behaves as a nonlinear fluorophore with a clear upconverted fluorescence upon two-photon absorption. Excitation in the 700–950 nm region with a femtosecond laser with a high excitation power density (1 MW cm^{-2}) causes the simultaneous absorption of two NIR-photons leading to emission at higher energies (500–700 nm, Fig. 4). The emission spectrum induced by excitation with two-photons of 770 nm (TPE in Fig. 4b, red dash line) is exactly coincident with the one induced by a single photon of 353 nm (OPE in Fig. 4b, black line). The TPA maximum appears at *ca.* 760 nm with a cross-section (σ_2) of 130 GM resulting in a two-photon brightness ($\sigma_2\phi$) of 17 GM (Fig. 4a, red dash line). Although moderate, the TPA value is remarkable considering the distortion from planarity, required for inducing chiroptical properties, of **1** and the lack of electronic coupling effects observed in branched push–pull structures.[23] Importantly, no net absorption above 600 nm was observed in the linear absorption spectrum. Moreover, TPE was recorded with different incident power confirming the quadratic dependence of the upconverted emission on the excitation power (Fig. 4c). It is noteworthy that the TPA maximum appears shifted to higher energy transitions when compared with the OPA maximum. The calculations show that the four lowest energy transitions are all described by a redistribution of the electron density within the sp^2 core with a minor charge transfer to the helicene (see ESI, Table S5 and Fig. S29†). On the other hand, the strongest charge transfer occurs for higher energy transitions increasing the TPA probability. Namely, the transitions predicted at 380 and 397 nm that involve charge transfer between the helicene and the heptagon and the 385 nm transition involving an electron density transfer from the sp^2 core to the heptagon.

Chiroptical properties

Encouraged by the good optical properties of **1**, we aimed to study its chiroptical properties. To this end, **1** bears bulky ^{t}Bu groups at the [5]helicene region to allow chiral resolution of each enantiomer *M*-**1** and *P*-**1**. Both enantiomers were separated and isolated by semipreparative chiral HPLC. We determined the Gibbs activation energy ($\Delta G^{\ddagger}$ (T)) for the racemization process by following the decay of the enantiomeric excess over time at different temperatures, resulting in $\Delta G^{\ddagger}$ (298 K) = 33.0 kcal mol^{-1} K^{-1} ($\Delta H^{\ddagger}$ = 32.1 kcal mol^{-1}, $\Delta S^{\ddagger}$ = −3 cal mol^{-1}, see ESI† for details), in the range of values recently reported by Juríček for [5]helicenes difunctionalized in the fjord region, and ensuring stability towards racemization at room temperature.[16]

The circular dichroism (CD) spectra of both enantiomers are depicted in Fig. 5a. We based our stereochemical assignment on TD-DFT calculations on the geometry of both enantiomers *M* and *P*-**1**. In agreement with the calculations, we correlate the main features of the CD spectrum observed as positive bands at 370, 385 and 475 nm and negative CD band at 498 nm with the *P*-**1** enantiomer (see ESI, Fig. S19 and Table S5†). The absolute

configuration of simple [*n*]helicenes has been usually related with the sign of the first intense band at the longest wavelength of the CD spectra.[24a] Nevertheless, CD bands corresponding to minor absorption bands due to the presence of substituents show shapes and signs strongly dependent of the global structure. Moreover, vibronic contributions can also determine the sign of the observed bands.[24b] It is noteworthy that the sign of the longest wavelength CD band, even if it is a low intense one, usually determines the sign of the CPL spectrum. Taking into account the presence of a very weak absorption band at 555 nm, we increased the concentration up to 10^{-3} M, thus being able to observe the corresponding CD band (Fig. 5a, inset). The dissymmetry value g_{abs} of **1** in CH_2Cl_2 ranged from 2.7×10^{-3} at 370 nm to 5.3×10^{-4} at 555 nm.

The bands observed below 400 nm are dominated by transitions from the H and H + 1 orbitals to the L and L + 1 orbitals (see ESI, Fig. S29† for a description of the molecular orbitals). All this transitions are localized in the sp^2 core and shows a significant contribution from the chiral moiety (the L + 1 orbital is clearly centered at the helicene). The strong bands in the 350–400 nm region in the CD spectrum (calculated at 397 nm and 380 nm) involve the charge transfer between the helicene and the heptagon units (see ESI, Table S5 and Fig. S30†). Interestingly, these are also the transitions that appear to be more active in the two-photon absorption spectrum. Therefore, the presence of the heptagon unit and the possibility of having a charge transfer between the chiral moiety and the heptagon favour both the CD response and the two-photon absorption.

We also recorded the circularly polarized luminescence (CPL) spectra of *M*-**1** and *P*-**1** (Fig. 5b) at 10^{-5} M in CH_2Cl_2, thus discarding the formation of aggregates that would lead to artifact signals due to photoselection.[25] As expected, the CPL spectrum showed an emission maxima at 560 nm upon irradiation with UV light (λ_{exc} = 372 nm) whose sign correlates with the lowest energy CD sign (band at 555 nm). Remarkably, CPL emission maxima matches the same energy transition observed for the upconverted emission upon two-photon absorption (λ_{exc} = 770 nm), which would represent an unprecedented process of TPA-based upconverted CPL. We evaluated the g_{lum} value as 2.3×10^{-4} for **1** which, to the best of our knowledge represents the first reported circularly polarized emission for an enantiopure nanographene. Unfortunately the comparison between the optical properties of **1** with those of a model heptagon-free compound was not possible as, in our hands, the synthesis of a purely hexagonal model compound with similar length and width incorporating a [5]helicene subunit led to a complex mixture of compounds which could not be purified and characterized properly. In this case, the distortion caused by the [5]helicene subunit and the presence of the ^{t}Bu groups are not sufficient to confer the necessary processability and solubility to the model compound. The dipole moment created by the tropone moiety seems to be mandatory for the processability of the model compound that has a lower estimated dipole moment (1.02 D) when compared with compound **1**.

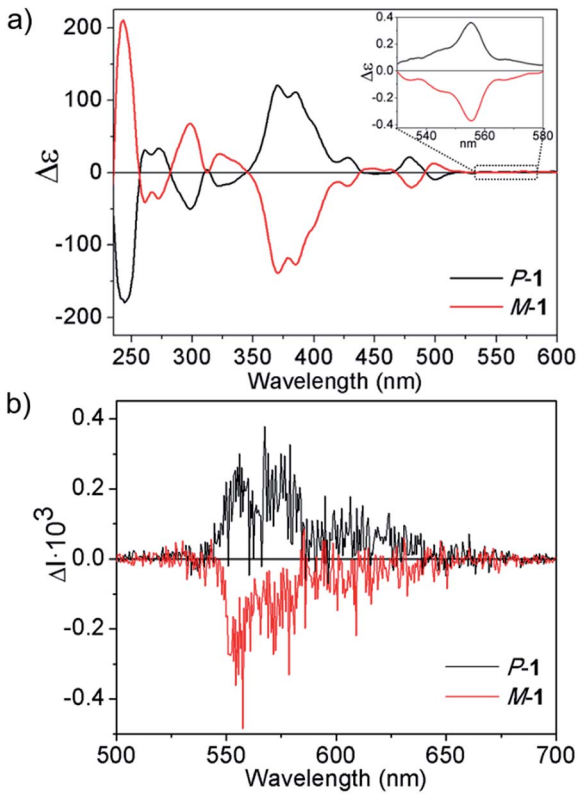

Fig. 5 (a) CD spectra of *M*-**1** and *P*-**1** at 10^{-5} M in CH_2Cl_2. Inset: CD spectra of *M*-**1** and *P*-**1** in the 530–580 nm region at 10^{-3} M in CH_2Cl_2. (b) CPL spectra of *M*-**1** and *P*-**1** at 10^{-5} M in CH_2Cl_2 upon excitation at 372 nm.

Electrochemical properties

The good solubility of **1** in organic solvents allowed us to also evaluate its electrochemical behavior. Cyclic voltammetry (CV) (1 mM, ^{n}Bu$_4$NPF$_6$, in THF) showed reversible reduction peaks at −2.06 and −2.37 V and reversible oxidation peaks at 0.60 and 0.90 V *versus* Fc/Fc* (Fig. 6) (THF was used as solvent due to its large electrochemical window on the reduction process). Hence, the HOMO–LUMO energy gaps based on the first half-wave oxidation and reduction potentials resulted in 2.66 eV.

In situ spectroelectrochemical measurements showed the spectroscopic response of **1** during its oxidation/reduction. During a potential sweep, the new species generated exhibited significantly red-shifted absorption maxima at 710 and 680 nm upon oxidation and reduction, respectively, drastically

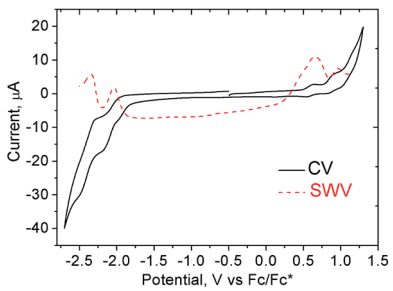

Fig. 6 Cyclic (CV) and square wave (SWV) voltammograms of **1** (1 mM) in THF (internal standard Fc/Fc*, v = 0.1 V s^{-1}).

diminishing the optical band gaps down to 1.74 eV upon oxidation and to 1.82 eV upon reduction. Moreover, the oxidized specie was relatively stable as we could generate it chemically by addition of tris(4-bromophenyl)ammoniumyl hexachloroantimonate (commonly known as "magic blue")[26] showing also the red-shifted absorption maxima. The ^{1}H NMR of a solution of **1** upon addition of "magic blue" (1 equiv.) showed a peak broadening as expected for the formation of radical species (see ESI, Fig. S23 to S25†).

The NIR absorption maxima together with their chiroptical properties and stability would make these oxidized species promising materials for optoelectronic devices.

On-surface study

In order to study the behavior of this nanographene on a substrate, we carried out preliminary experiments to test the feasibility to deposit this large molecule on a single crystal surface under high or ultra-high vacuum (HV/UHV) conditions. Thermal in-vacuum sublimation of **1** is a challenge due to its high molecular weight, which prevents their evaporation before partial or total decomposition. However, we succeeded in depositing submonolayer coverage of **1** on Cu(111) by means of a pulsed-injection device (see ESI for details, Fig. S31†).[27] Room temperature scanning tunneling microscopy (RT-STM) images of the Cu(111) surface before and after deposition of **1** clearly show that the Cu surface is covered by homogeneously distributed features with elongated shape and approximate dimensions of 2.3 nm and 1.3 nm along both in-plane axis, and 1.8 Å of apparent height. The good agreement between the dimensions obtained from STM and those extracted from X-ray crystallography, together with the control experiments, allow us to assign these features to the nanographene molecule **1** (see ESI, Fig. S31c†), and shows that the deposition of such large, curved compounds under HV/UHV conditions is possible.

Conclusions

In conclusion, we have showed that the introduction of defects can lead to unprecedented properties in polyaromatic hydrocarbons in terms of solubility and optical properties. The introduction of one tropone moiety in a ribbon-shaped nanographene allows the induction of a push–pull effect favouring the non-linear optical response (*i.e.* TPA and TPE). In addition, the presence of a chiral moiety such as a carbohelicene in the π-extended aromatic backbone induces chiroptical responses (*i.e.* CD and CPL). Thus, enantiopure distorted ribbon-shaped graphene molecule **1** constitutes the first example of an organic compound in which both TPA-based upconversion (UC-TPA) and CPL are reported to date. More importantly, both upconversion and CPL responses have a common origin in the excitation of transitions involving the tropone and the [5]helicene moiety. Although moderate, noteworthy, we present the first reported circularly polarized emission g_{lum} value for an enantiopure nanographene. Finally, we have shown that it is feasible to deposit aromatic saddles as **1** under HV/UHV conditions on a Cu(111) single crystal, thus opening a door towards atomic characterization of related distorted and curved PAHs by Surface Science techniques.

Conflicts of interest

There are no conflicts to declare.

Acknowledgements

This project has received funding from the European Research Council (ERC) under the European Union's Horizon 2020 research and innovation program (ERC-2015-STG-677023). We also thank the Ministerio de Economía y Competitividad (MINECO, Spain) (CTQ2015-70283-P, CTQ2014-53598-R, MAT2014-54231-C4-1P, FIS2016-77578-R) and the "Unidad de Excelencia Química Aplicada a Biomedicina y Medioambiente (UGR)". A. G. C., C. S. S. and C. M. C. acknowledge funding from MINECO (Spain) for RyC-2013-12943, IJCI-2014-19291 and BES-2016-076371 contracts, respectively. I. R. M. thanks UGR (Spain) for a postdoctoral scholarship. I. M. and E. M. thank the Fundação para a Ciência e a Tecnologia for financial support (IF/00759/2013 and post-doc grant SFRH/BPD/75782/2011). We thank the CSIRC-Alhambra for supercomputing facilities.

Notes and references

1 (*a*) A. Eftekhari and H. Garcia, *Mater Today Chem.*, 2017, **4**, 1–16; (*b*) J. T. Robinson, M. K. Zalalutdinov, C. D. Cress, J. C. Culbertson, A. L. Friedman, A. Merrill and B. J. Landi, *ACS Nano*, 2017, **11**, 4745–4752.

2 (*a*) L. Li, G. Wu, G. Yang, J. Peng, J. Zhao and J. J. Zhu, *Nanoscale*, 2013, **5**, 4015–4039; (*b*) S. Zhu, Y. Song, X. Zhao, J. Shao, J. Zhang and B. Yang, *Nano Res.*, 2015, **8**, 355–381; (*c*) Z. Gan, H. Xu and Y. Hao, *Nanoscale*, 2016, **8**, 7794–7807.

3 (*a*) Q. Liu, B. Guo, Z. Rao, B. Zhang and J. R. Gong, *Nano Lett.*, 2013, **13**, 2436–2441; (*b*) M. Lan, S. Zhao, Z. Zhang, L. Yan, L. Guo, G. Niu, J. Zhang, J. Zhao, H. Zhang, P. Wang, G. Zhu, C.-S. Lee and W. Zhang, *Nano Res.*, 2017, **10**, 3113–3123.

4 (*a*) M. Pawlicki, H. A. Collins, R. G. Denning and H. L. Anderson, *Angew. Chem., Int. Ed.*, 2009, **48**, 3244–3266; (*b*) E. Maçôas, G. Marcelo, S. Pinto, T. Caneque, A. M. Cuadro, J. J. Vaquero and J. M. Martinho, *Chem. Commun.*, 2011, **47**, 7374–7376; (*c*) L. Guo and M. S. Wong, *Adv. Mater.*, 2014, **26**, 5400–5428; (*d*) I. F. A. Mariz, F. Siopa, C. A. B. Rodrigues, C. A. M. Afonso, X. Chen, J. M. G. Martinho and E. M. S. Maçôas, *J. Mater. Chem. C*, 2015, **3**, 10775–10782.

5 (*a*) K. A. Ritter and J. W. Lyding, *Nat. Mater.*, 2009, **8**, 235–242; (*b*) L.-s. Li and X. Yan, *J. Phys. Chem. Lett.*, 2010, **1**, 2572–2576; (*c*) N. Fuyuno, D. Kozawa, Y. Miyauchi, S. Mouri, R. Kitaura, H. Shinohara, T. Yasuda, N. Komatsu and K. Matsuda, *Adv. Opt. Mater.*, 2014, **2**, 983–989; (*d*) F. Arcudi, L. Dordevic and M. Prato, *Angew. Chem., Int. Ed.*, 2016, **55**, 2107–2112.

6 (*a*) L. T. Scott, M. M. Boorum, B. J. McMahon, S. Hagen, J. Mack, J. Blank, H. Wegner and A. de Meijere, *Science*, 2002, **295**, 1500–1503; (*b*) Y.-T. Wu and J. S. Siegel, *Chem.*

Rev., 2006, **106**, 4843–4867; (*c*) J. Wu, W. Pisula and K. Müllen, *Chem. Rev.*, 2007, **107**, 718–747; (*d*) L. Chen, Y. Hernandez, X. Feng and K. Müllen, *Angew. Chem., Int. Ed.*, 2012, **51**, 7640–7654; (*e*) A. Narita, X. Feng, Y. Hernandez, S. A. Jensen, M. Bonn, H. Yang, I. A. Verzhbitskiy, C. Casiraghi, M. R. Hansen, A. H. Koch, G. Fytas, O. Ivasenko, B. Li, K. S. Mali, T. Balandina, S. Mahesh, S. De Feyter and K. Müllen, *Nat. Chem.*, 2014, **6**, 126–132; (*f*) A. Narita, X. Feng and K. Müllen, *Chem. Rec.*, 2015, **15**, 295–309.

7 (*a*) X. Li, X. Wang, L. Zhang, S. Lee and H. Dai, *Science*, 2008, **319**, 1229–1232; (*b*) D. V. Kosynkin, A. L. Higginbotham, A. Sinitskii, J. R. Lomeda, A. Dimiev, B. K. Price and J. M. Tour, *Nature*, 2009, **458**, 872–876.

8 E. E. Maroto, M. Izquierdo, S. Reboredo, J. Marco-Martínez, S. Filippone and N. Martin, *Acc. Chem. Res.*, 2014, **47**, 2660–2670.

9 Two example showing CPL and upconversion based on an alternative triplet–triplet annihilation process have been recently described: (*a*) P. Duan, D. Asthana, T. Nakashima, T. Kawai, N. Yanai and N. Kimizuka, *Faraday Discuss.*, 2017, **196**, 305–316; (*b*) J. Han, P. Duan, X. Li and M. Liu, *J. Am. Chem. Soc.*, 2017, **139**, 9783–9786.

10 (*a*) M. Albota, D. Beljonne, J.-L. Brédas, J. E. Ehrlich, J.-Y. Fu, A. A. Heikal, S. E. Hess, T. Kogej, M. D. Levin, S. R. Marder, D. McCord-Maughon, J. W. Perry, H. Röckel, M. Rumi, G. Subramaniam, W. W. Webb, X.-L. Wu and C. Xu, *Science*, 1998, **281**, 1653–1656; (*b*) M. Rumi, J. E. Ehrlich, A. A. Heikal, J. W. Perry, S. Barlow, Z. Hu, D. McCord-Maughon, T. C. Parker, H. Röckel, S. Thayumanavan, S. R. Marder, D. Beljonne and J.-L. Brédas, *J. Am. Chem. Soc.*, 2000, **122**, 9500–9510; (*c*) I. F. A. Mariz, E. M. S. Maçôas, J. M. G. Martinho, L. Zou, P. Zhou, X. Chen and J. Qin, *J. Mater. Chem. B*, 2013, **1**, 2169–2177; (*d*) G. Marcelo, S. Pinto, T. Caneque, I. F. Mariz, A. M. Cuadro, J. J. Vaquero, J. M. Martinho and E. M. Macoas, *J. Phys. Chem. A*, 2015, **119**, 2351–2362.

11 (*a*) E. M. Sanchez-Carnerero, A. R. Agarrabeitia, F. Moreno, B. L. Maroto, G. Muller, M. J. Ortiz and S. de la Moya, *Chem.–Eur. J.*, 2015, **21**, 13488–13500; (*b*) J. Kumar, T. Nakashima and T. Kawai, *J. Phys. Chem. Lett.*, 2015, **6**, 3445–3452; (*c*) G. Longhi, E. Castiglioni, J. Koshoubu, G. Mazzeo and S. Abbate, *Chirality*, 2016, **28**, 696–707.

12 Applications in CPL LEDs have been reported: (*a*) F. Zinna, U. Giovanella and L. Di Bari, *Adv. Mater.*, 2015, **27**, 1791–1795; (*b*) J. R. Brandt, X. Wang, Y. Yang, A. J. Campbell and M. J. Fuchter, *J. Am. Chem. Soc.*, 2016, **138**, 9743–9746.

13 For recent examples of helicene-based CPL-active compounds: (*a*) K. Nakamura, S. Furumi, M. Takeuchi, T. Shibuya and K. Tanaka, *J. Am. Chem. Soc.*, 2014, **136**, 5555–5558; (*b*) C. Shen, E. Anger, M. Srebro, N. Vanthuyne, K. K. Deol, T. D. Jefferson, G. Muller, J. A. G. Williams, L. Toupet, C. Roussel, J. Autschbach, R. Réau and J. Crassous, *Chem. Sci.*, 2014, **5**, 1915–1927; (*c*) S. Abbate, G. Longhi, F. Lebon, E. Castiglioni, S. Superchi, L. Pisani, F. Fontana, F. Torricelli, T. Caronna, C. Villani, R. Sabia, M. Tommasini, A. Lucotti, D. Mendola, A. Mele and D. A. Lightner, *J. Phys. Chem. C*, 2014, **118**, 1682–1695; (*d*) T. Matsuno, Y. Koyama, S. Hiroto, J. Kumar, T. Kawai and H. Shinokubo, *Chem. Commun.*, 2015, **51**, 4607–4610; (*e*) N. Saleh, M. Srebro, T. Reynaldo, N. Vanthuyne, L. Toupet, V. Y. Chang, G. Muller, J. A. Williams, C. Roussel, J. Autschbach and J. Crassous, *Chem. Commun.*, 2015, **51**, 3754–3757; (*f*) S. Feuillastre, M. Pauton, L. Gao, A. Desmarchelier, A. J. Riives, D. Prim, D. Tondelier, B. Geffroy, G. Muller, G. Clavier and G. Pieters, *J. Am. Chem. Soc.*, 2016, **138**, 3990–3993; (*g*) I. H. Delgado, S. Pascal, A. Wallabregue, R. Duwald, C. Besnard, L. Guénée, C. Nançoz, E. Vauthey, R. C. Tovar, J. L. Lunkley, G. Muller and J. Lacour, *Chem. Sci.*, 2016, **7**, 4685–4693; (*h*) H. Sakai, T. Kubota, J. Yuasa, Y. Araki, T. Sakanoue, T. Takenobu, T. Wada, T. Kawai and T. Hasobe, *J. Phys. Chem. C*, 2016, **120**, 7860–7869; (*i*) N. Hellou, M. Srebro-Hooper, L. Favereau, F. Zinna, E. Caytan, L. Toupet, V. Dorcet, M. Jean, N. Vanthuyne, J. A. G. Williams, L. Di Bari, J. Autschbach and J. Crassous, *Angew. Chem., Int. Ed.*, 2017, **56**, 8236–8239; (*j*) K. Murayama, Y. Shibata, H. Sugiyama, H. Uekusa and K. Tanaka, *J. Org. Chem.*, 2017, **82**, 1136–1144; (*k*) H. Nishimura, K. Tanaka, Y. Morisaki, Y. Chujo, A. Wakamiya and Y. Murata, *J. Org. Chem.*, 2017, **82**, 5242–5249; (*l*) K. Dhbaibi, L. Favereau, M. Srebro-Hooper, M. Jean, N. Vanthuyne, F. Zinna, B. Jamoussi, L. Di Bari, J. Autschbach and J. Crassous, *Chem. Sci.*, 2018, **9**, 735–742. For a CPL-active π-extended binaphtyl analogue see: (*m*) Y. Uchida, T. Hirose, T. Nakashima, T. Kawai and K. Matsuda, *Org. Lett.*, 2016, **18**, 2118–2121.

14 Other heptagon-containing polycyclic arenes: (*a*) K. Yamamoto, T. Harada and M. Nakazaki, *J. Am. Chem. Soc.*, 1983, **105**, 7171–7172; (*b*) K. Yamamoto, T. Harada, Y. Okamoto, H. Cbikamatsu, M. Nakazaki, Y. Kai, T. Nakao, M. Tanaka, S. Harada and N. Kasai, *J. Am. Chem. Soc.*, 1988, **110**, 3578–3584; (*c*) K. Yamamoto, H. Sonobe, H. Matsubara, M. Sato, S. Okamoto and K. Kitaura, *Angew. Chem., Int. Ed.*, 1996, **35**, 69–70; (*d*) J. Luo, X. Xu, R. Mao and Q. Miao, *J. Am. Chem. Soc.*, 2012, **134**, 13796–13803; (*e*) E. U. Mughal and D. Kuck, *Chem. Commun.*, 2012, **48**, 8880–8882; (*f*) K. Kawasumi, Q. Zhang, Y. Segawa, L. T. Scott and K. Itami, *Nat. Chem.*, 2013, **5**, 739–744; (*g*) A. Pradhan, P. Dechambenoit, H. Bock and F. Durola, *J. Org. Chem.*, 2013, **78**, 2266–2274; (*h*) E. U. Mughal, B. Neumann, H.-G. Stammler and D. Kuck, *Eur. J. Org. Chem.*, 2014, 7469–7480; (*i*) K. Y. Cheung, X. Xu and Q. Miao, *J. Am. Chem. Soc.*, 2015, **137**, 3910–3914; (*j*) Q. Miao, *Chem. Rec.*, 2015, **15**, 1156–1159; (*k*) K. Kato, Y. Segawa, L. T. Scott and K. Itami, *Chem.–Asian J.*, 2015, **10**, 1635–1639; (*l*) H. W. Ip, C. F. Ng, H. F. Chow and D. Kuck, *J. Am. Chem. Soc.*, 2016, **138**, 13778–13781; (*m*) H.-W. Ip, H.-F. Chow and D. Kuck, *Org. Chem. Front.*, 2017, **4**, 817–822; (*n*) S. Nobusue, K. Fujita and Y. Tobe, *Org. Lett.*, 2017, **19**, 3227–3230; (*o*) N. Fukui, T. Kim, D. Kim and A. Osuka, *J. Am. Chem. Soc.*, 2017, **139**, 9075–9088; (*p*) T. Fujikawa, Y. Segawa and K. Itami, *J. Org. Chem.*, 2017, **82**, 7745–7749; (*q*) X. Gu, H. Li, B. Shan, Z. Liu and Q. Miao, *Org. Lett.*, 2017, **19**,

2246–2249; (*r*) W. S. Wong, C. F. Ng, D. Kuck and H. F. Chow, *Angew. Chem., Int. Ed.*, 2017, **56**, 12356–12360; (*s*) S. H. Pun, C. K. Chan, J. Luo, Z. Liu and Q. Miao, *Angew. Chem., Int. Ed.*, 2018, **57**, 1581–1586.

15 For theoretical studies on the influence of the presence of seven-membered rings on the properties see: (*a*) X. Wang, S. Yu, Z. Lou, Q. Zeng and M. Yang, *Phys. Chem. Chem. Phys.*, 2015, **17**, 17864–17871; (*b*) M. Hatanaka, *J. Phys. Chem. A*, 2016, **120**, 1074–1083; (*c*) Y. Dai, Z. Li and J. Yang, *Carbon*, 2016, **100**, 428–434.

16 P. Ravat, R. Hinkelmann, D. Steinebrunner, A. Prescimone, I. Bodoky and M. Juríček, *Org. Lett.*, 2017, **19**, 3707–3710.

17 I. R. Márquez, N. Fuentes, C. M. Cruz, V. Puente-Muñoz, L. Sotorrios, M. L. Marcos, D. Choquesillo-Lazarte, B. Biel, L. Crovetto, E. Gómez-Bengoa, M. T. González, R. Martin, J. M. Cuerva and A. G. Campaña, *Chem. Sci.*, 2017, **8**, 1068–1074.

18 Reviews on helicenes: (*a*) Y. Shen and C. F. Chen, *Chem. Rev.*, 2012, **112**, 1463–1535; (*b*) M. Gingras, *Chem. Soc. Rev.*, 2013, **42**, 968–1006; (*c*) M. Gingras, G. Felix and R. Peresutti, *Chem. Soc. Rev.*, 2013, **42**, 1007–1050; (*d*) M. Gingras, *Chem. Soc. Rev.*, 2013, **42**, 1051–1095; (*e*) M. Rickhaus, M. Mayor and M. Juríček, *Chem. Soc. Rev.*, 2016, **45**, 1542–1556.

19 For other related helical π-extended aromatic systems see: (*a*) D. Peña, D. Pérez, E. Guitián and L. Castedo, *Org. Lett.*, 1999, **1**, 1555–1557; (*b*) X. Feng, J. Wu, V. Enkelmann and K. Müllen, *Org. Lett.*, 2006, **8**, 1145–1148; (*c*) R. A. Pascal Jr, *Chem. Rev.*, 2006, **106**, 4809–4819; (*d*) S. Xiao, S. J. Kang, Y. Wu, S. Ahn, J. B. Kim, Y.-L. Loo, T. Siegrist, M. L. Steigerwald, H. Li and C. Nuckolls, *Chem. Sci.*, 2013, **4**, 2018; (*e*) T. Fujikawa, Y. Segawa and K. Itami, *J. Am. Chem. Soc.*, 2015, **137**, 7763–7768; (*f*) L. Shan, D. Liu, H. Li, X. Xu, B. Shan, J. B. Xu and Q. Miao, *Adv. Mater.*, 2015, **27**, 3418–3423; (*g*) X. Geng, J. P. Donahue, J. T. Mague and R. A. Pascal Jr, *Angew. Chem., Int. Ed.*, 2015, **54**, 13957–13960; (*h*) X. Y. Wang, X. C. Wang, A. Narita, M. Wagner, X. Y. Cao, X. Feng and K. Müllen, *J. Am. Chem. Soc.*, 2016, **138**, 12783–12786; (*i*) N. J. Schuster, D. W. Paley, S. Jockusch, F. Ng, M. L. Steigerwald and C. Nuckolls, *Angew. Chem., Int. Ed.*, 2016, **55**, 13519–13523; (*j*) T. Fujikawa, D. V. Preda, Y. Segawa, K. Itami and L. T. Scott, *Org. Lett.*, 2016, **18**, 3992–3995; (*k*) T. Fujikawa, Y. Segawa and K. Itami, *J. Am. Chem. Soc.*, 2016, **138**, 3587–3595; (*l*) Y. Yang, L. Yuan, B. Shan, Z. Liu and Q. Miao, *Chem.–Eur. J.*, 2016, **22**, 18620–18627; (*m*) Y. Zhong, T. J. Sisto, B. Zhang, K. Miyata, X. Y. Zhu, M. L. Steigerwald, F. Ng and C. Nuckolls, *J. Am. Chem. Soc.*, 2017, **139**, 5644–5647; (*n*) M. Daigle, D. Miao, A. Lucotti, M. Tommasini and J. F. Morin, *Angew. Chem., Int. Ed.*, 2017, **56**, 6213–6217; (*o*) T. J. Sisto, Y. Zhong, B. Zhang, M. T. Trinh, K. Miyata, X. Zhong, X. Y. Zhu, M. L. Steigerwald, F. Ng and C. Nuckolls, *J. Am. Chem. Soc.*, 2017, **139**, 5648–5651; (*p*) W. Yang, G. Longhi, S. Abbate, A. Lucotti, M. Tommasini, C. Villani, V. J. Catalano, A. O. Lykhin, S. A. Varganov and W. A. Chalifoux, *J. Am. Chem. Soc.*, 2017, **139**, 13102–13109; (*q*) V. Berezhnaia, M. Roy, N. Vanthuyne, M. Villa, J.-V. Naubron, J. Rodriguez, Y. Coquerel and M. Gingras, *J. Am. Chem. Soc.*, 2017, **139**, 18508–18511; (*r*) T. Hosokawa, Y. Takahashi, T. Matsushima, S. Watanabe, S. Kikkawa, I. Azumaya, A. Tsurusaki and K. Kamikawa, *J. Am. Chem. Soc.*, 2017, **139**, 18512–18521.

20 Single crystals of minor compound **6** were also obtained, showing similar features, see ESI† for further details.

21 W. E. Acree, A. I. Zvaigzne and J. C. Fetzer, *Appl. Spectrosc.*, 1990, **44**, 1193–1195.

22 F. Wurthner, *Chem. Commun.*, 2004, 1564–1579.

23 (*a*) Z. Zeng, Z. Guan, Q.-H. Xu and J. Wu, *Chem.–Eur. J.*, 2011, **17**, 3837–3841; (*b*) Reference standards for TPA from: S. de Reguardati, J. Pahapill, A. Mikhailov, Y. Stepanenko and A. Rebane, *Opt. Express*, 2015, **24**, 9053–9066.

24 (*a*) F. Furche, R. Ahlrichs, C. Wachsmann, E. Weber, A. Sobanski, F. Vögtle and S. Grimme, *J. Am. Chem. Soc.*, 2000, **122**, 1717–1724; (*b*) S. Abbate, G. Longhi, F. Lebon, E. Castiglioni, S. Superchi, L. Pisani, F. Fontana, F. Torricelli, T. Caronna, C. Villani, R. Sabia, M. Tommasini, A. Lucotti, D. Mendola, A. Mele and D. A. Lightner, *J. Phys. Chem. C*, 2014, **118**, 1682–1695.

25 (*a*) H. Tanaka, Y. Inoue and T. Mori, *ChemPhotoChem*, 2018, DOI: 10.1002/cptc.201800015; (*b*) Circular polarization was also confirmed by looking at the signal at a frequency of 2 × 50 kHz, as 50 kHz is the frequency of the PEM acting as an oscillating quarter-wave plate in our equipment: H. P. J. M. Dekkers, P. F. Moraal, J. M. Timper and J. P. Riehl, *Appl. Spectrosc.*, 1985, **39**, 818–821.

26 N. G. Connelly and W. E. Geiger, *Chem. Rev.*, 1996, **96**, 877–910.

27 J. M. Sobrado and J. A. Martín-Gago, *J. Appl. Phys.*, 2016, **120**, 145307.